scientific reports

Check for updates

OPEN

Assessing climate change impacts on flood risk in the Yeongsan River Basin, South Korea

Agbortoko Bate Ashu[1] & Junsuk Kang[2,3,4,5]✉

Flood risk prediction is critical for adaptation to the forecast frequency of extreme weather events. As South Korea experiences events that cause widespread flood damage, we conducted a flood risk assessment by employing global climate models and a hydrological model of the Yeongsan River Basin. Using shared socioeconomic pathway scenario data from the soil and water assessment tool, we simulated daily streamflow and reservoir outflow data for each sub-basin, modeling baseline, mid-century, and end-century scenarios. Four flood indices (duration, magnitude, probability, and frequency) were used for estimating flood risk. The spatial distribution of flood risk projected higher risks in most sub-basins for the mid- and end-century scenarios with an increase of flood amount to about 65% in the future. Adaptive strategies were required to address the risks of both flash floods and longer-term flooding. The study facilitates prioritizing flood risk regions for implementing effective preventive measures and efficient flood management.

Climate change is projected to cause more frequent and heavy rainfall events and increased temperatures in the future, as well as changes in the spatiotemporal patterns of precipitation and temperature[1]. Floods are a prevalent and devastating category of natural disasters that annually cause countless fatalities worldwide[2,3]. South Korea has a tropical monsoon climate that renders the country vulnerable to climate change. The region receives 68% of total precipitation in June–September, and notable variations in precipitation patterns could indicate a higher risk of flooding or drought[4]. Typhoons and intense rainfall cause widespread flooding damage in South Korea every two years[5,6]. Mitigating flood risk in agricultural watersheds requires the establishment of appropriate flood risk measures, such as hazard analysis[7]. Hazard analyses require future climate change data to evaluate flood hazards based on historical data[8–11]. Various approaches are used in estimating climate extremes that cause flooding, such as investigating their frequency, magnitude, duration, exceedance, or variability[12–16].

Regional climate models and global climate models (RCMs and GCMs, respectively), have long been used to estimate potential future responses to changing circumstances[17]. Several hydrological studies have used GCM and RCM data to project the implications of climate change up to 2100 for representative concentration pathways (RCPs) of greenhouse gases. Previous climate change scenarios such as SA90 and SRES from the Intergovernmental Panel on Climate Change (IPCC) considered only rainfall, energy structures, and temperature[18]. However, the IPCC 6th Assessment Report indicate five shared socioeconomic pathways (SSPs) for future socially sustainable development scenarios[19,20]. The SSPs link indicators of socioeconomic development, such as GDP, population, and urbanization to the CO_2 concentration target[21]. The GCMs indicate a higher chance of future flooding along with rising temperatures, leading to uncertainty in obtaining accurate flood risk assessment results[22,23]. Selecting a suitable GCM is essential for quantifying future flood risks associated with climate change adaptation. Bias correction and statistical downscaling methods (SDM) in obtaining climate data at finer spatial scales in assessing future local impacts of climate change[24–26]. Several statistical downscaling methods have been developed and examined to assess the impacts of climate change[27]. The demand for high-resolution spatiotemporal data in hydrological impact assessments of climate change has led to a growing reliance on statistical downscaling methods[28,29].

Routing future climate data with hydrological models, such as TOPMODEL, HEC-RAS, MIKESHE, HEC-HMS, SWMM, FLO-2D, and the Soil and Water Assessment Tool (SWAT) facilitates the evaluation of local and regional flood risks[30–32]. Hydrological models coupled with GCMs are essential for quantifying future flood

[1]Research Center for Regional Climate Crisis Response, Seoul National University, Seoul 08826, Korea. [2]Interdisciplinary Program in Landscape Architecture, Seoul National University, Seoul 08826, Korea. [3]Transdisciplinary Program in Smart City Global Convergence, Seoul National University, Seoul 08826, Korea. [4]Department of Landscape Architecture and Rural Systems Engineering, Seoul National University, Seoul 08826, Korea. [5]Research Institute of Agriculture and Life Sciences, Seoul National University, Seoul 08826, Korea. ✉email: windkplus@hotmail.com

risks. The SWAT model with GCMs has been used to determine the effects of climate change on flood risk[30]. As the SWAT model offers substantial accessibility and easy input data management, significant applications have been developed in researching the effects of climate change and hydrological modelling[31–40]. The authors reported that declining rainfall and rising temperatures increased the relative hazard levels for future conditions. Flood frequency was evaluated with 21 GCMs using the SWAT model in Bitlis Creek, Turkey[39]. Results show that under SSP245 and SSP585 (2025–2099), flood discharges increased by 31.7% from the historical period (1955–2010). A comprehensive assessment of projected flood hazards across Vietnam under four SSPs and two periods (2036–2065 and 2070–2099) shows an increase in streamflow by 31% with a potential future flood risk using the SWAT model and 20 GCMs[40]. Dysarz et al.[41] evaluated future spatial extent and depth classes of flood hazard zones in the middle course of the River Warta, Poland using SWAT and HEC-RAS models. RCPs (4.5 and 8.5) for three return periods (10-, 100- and 500-year floods) from 2021 to 2050 indicate that the flood extend are projected to increase and the mean water depths of the flooded areas are projected to decrease with increase in flood inundated areas.

Several studies have been conducted in South Korea to predict severe floods using hydrological models and GCMs[42,43]. Son et al.[44] determined the likelihood of severe rainfall, related flood levels, and the flood volume of the Namhangang River using projected climate change data from 13 GCMs. The authors reported increases in the likelihood of severe rainfall, flood volume, and flood level occurrences of 13.0–15%, 29–33.5%, and 12.6–13.6%, respectively. Using xp-swmm software, Hwang et al.[42] examined the effects of climate change on flood-level design in the Hwajabae drainage basin of Korea. The findings highlight an increase in the peak flood volume, necessitating redesign of the urban drainage infrastructure to cope with severe floods. Kwak et al.[45] used the Hydrologic Modeling System (HEC-HMS) to assess the effects of rainfall distribution, curve number (CN), and climate change on flood volume variations in the Yedang watershed of Korea for RCP4.5/8.5 and SSP 2-4.5/5-8.5 scenarios. The findings indicate that between RCP 4.5/8.5 and SSP 2-4.5/5-8.5, the average flood volume would increase by 15% and 13%, respectively. Conventional watershed modelling approaches in Korea primarily focus on estimating flood volume and rainfall distribution in conjunction with Representative Concentration Pathway (RCP) scenarios. Despite advancements in modelling capabilities, many existing methods continue to rely on simplified indicators such as exceedance probability or spatial distribution patterns to assess flood risk. These approaches often fall short in capturing the complex dynamics of flood regimes. Numerous flood risk assessment studies in Korea have focused on the effects of climate change through a single flood characteristic, limiting the scope of their conclusions. However, integrating multiple flood characteristics is essential for accurately assessing future flood events and formulating effective flood risk management policies. As highlighted by Postel and Richter[46]comprehensive flow management should consider not only flood magnitude, but also duration and frequency. Moreover, accurate flood modelling must account for land use and key hydrological infrastructure, including dams, reservoirs, weirs, and drainage systems. Therefore, a flood hazard analysis framework that incorporates the impacts of climate change on multiple flood characteristics can significantly enhance flood risk assessment and management. In this study, a disaggregated flood hazard framework was used, separating recurrence probability, frequency, duration, and magnitude to provide a clearer, more actionable understanding of flooding patterns in Korea. Korea has experienced frequent flooding over the past decade, with the Yeongsan River Basin (YRB) being particularly vulnerable due to its high agricultural use (50%) and extensive dam and reservoir network (1,104 structures). Climate change, as projected by the SSP scenario, is expected to increase precipitation, heightening the risk of dam failures and overflows. Evaluating future flood risk is essential to identify high-risk areas and support adaptive planning and resilient infrastructure development to mitigate evolving flood threats. Accordingly, this study evaluated four flood risk hazard indices (duration, frequency, magnitude, and recurrence) to quantify future flood risk under SSP climate change scenarios in the YRB.

The YRB is located in the southwestern region of South Korea, covering 3441.09 km^2 (Fig. 1). It is the fourth largest basin in the country and the river is 129.5 km long. The YRB has Korea's largest agricultural land area, comprising 32% rice paddies, 34% forests, 18% upland crops, 1% grasslands, 2% bare fields, with 5% urban and 6% water areas[17,47]. The YRB supplies an average of three billion m^3 of water each year, accounting for approximately 3.9% of the total water resources in South Korea. The basin has 4 major agricultural dams, approximately 1102 small dams and reservoirs, 2 weirs, and a dyke used mostly for irrigation. Annual precipitation is 1391 mm in the monsoon watershed, and the average temperature is 14 °C. Summer monsoon rains in June–September account for approximately 60–70% of the total drainage[48,49].

This study evaluated the basin-level flood risk index linked with climate change. A developed, calibrated, and validated soil and SWAT hydrological model was used to assess the risk of future flooding in the region. The observed baseline (1980–2021) and future climate mid-century (2030–2060), and end-century (2070–2100) data from SSP scenarios were used as temperature and rainfall inputs for the SWAT model to simulate the daily streamflow and reservoir outflow for each sub-basin. An SSP scenario is essential for this study, as it links the CO_2 concentration target and socioeconomic development, such as GDP, population, socioeconomic changes, urbanization, as well as the radiative forcing intensity in 2100. Downscaling and bias corrections were applied to SSP scenario data. Streamflow and reservoir outflow output data from the SWAT model were processed in MATLAB® (MathWorks, Massachusetts, USA) to predict the flow rate for a 2-year return flood period. The simulated daily flow output was used as input to calculate flood hazard indices for each sub-basin under baseline and future climate change scenarios. The codes and detailed explanations used in this study derive from Cheng[50]. Future flood risk was assessed by conducting a comparative analysis of baseline and future scenarios in the YRB. Our findings are expected to provide adequate flood risk information to decision-makers and stakeholders concerned with the consequences and occurrences of flood events (Supplementary Data Fig. S1).

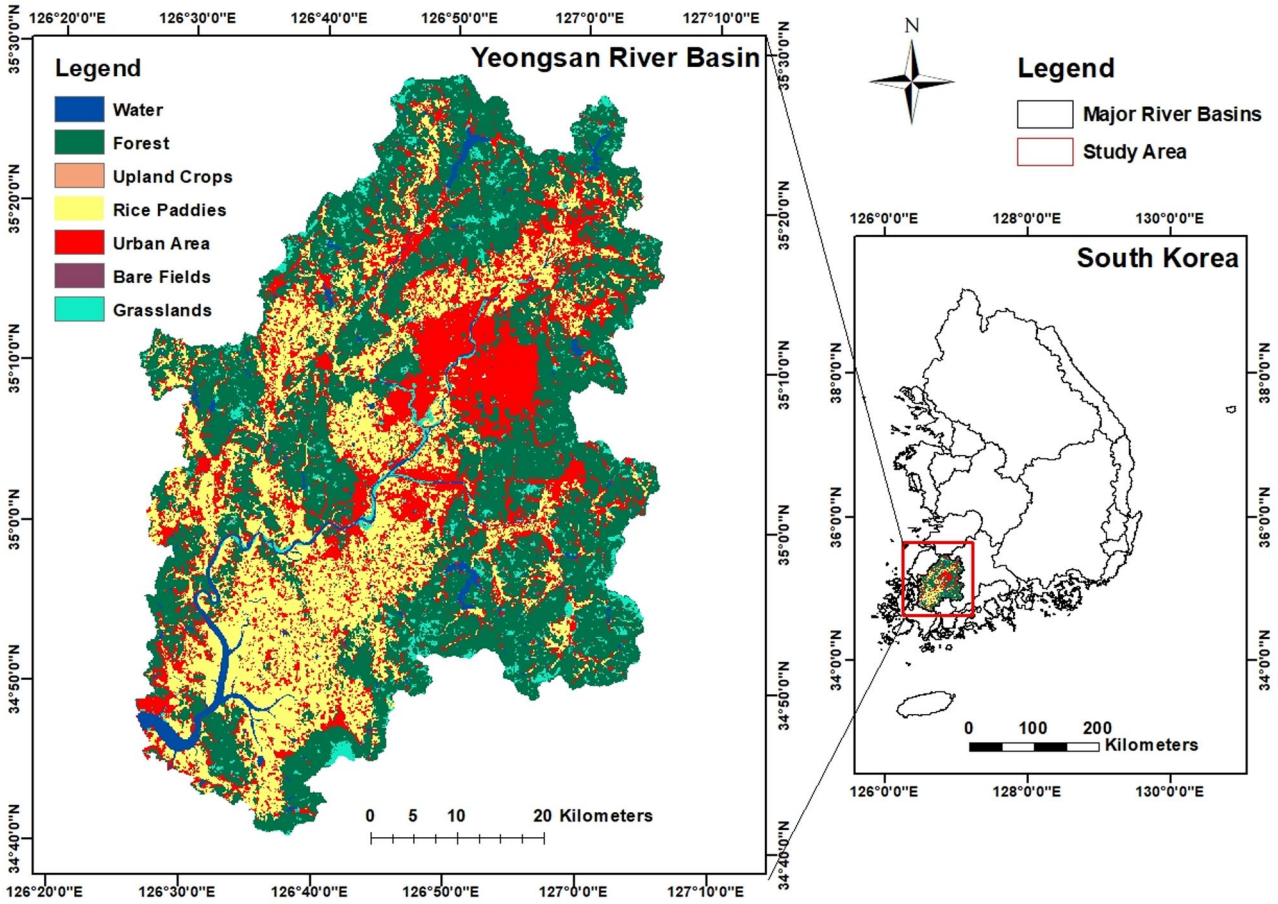

Fig. 1. The Yeongsan River Basin indicates landcover/use. The map shows the basin's extent and detailed land cover/use of the Basin.

Evaluation of the SWAT model

The SWAT model was calibrated (2006–2013) and validated (2014–2021) using observed and simulated data from four hydrological stations (S1, S2, S3, and S4) in the YRB at daily intervals. The sensitivity of the YRB SWAT model and calibrated parameters, performed by trial and error in SWAT-CUP, which directly influenced the streamflow are shown in Supplementary Data Table S5. Statistical analyses performed in this study included p-factor, r-factor, R^2·PBAIS, NSE, and RSR (Supplementary Data Fig. S2 and Supplemental Data Table. S1). The model's overall performance was 'satisfactory to very good' based on the criteria proposed by Moriasi et al.[51].

Projected changes in precipitation and temperature

Table 1 shows the monthly averages of precipitation, maximum temperature and minimum temperature for historical (1980–2023) and the four SSP scenarios (2024–2100). Historical average precipitation fluctuated between 1.09 mm in January (lowest precipitation) to 9.90 mm in July (Highest precipitation). Future scenarios show a decrease from the historical scenario in the month of July for all four scenarios with the least drop in the SSP3-7.0 scenario for the month of December (-1.23 mm) and the most decline in the SSP2-4.5 scenario for the month of January. The overall increase of precipitation across all the SSP scenarios indicating more precipitation amounts in the future which could lead to flooding.

Historical average maximum and minimum temperatures indicates that the lowest temperature occur in January and higher temperature in August. Future minimum temperature depicts in (Table 1). that the SSP1-2.6 scenario would have the lowest temperatures in March (-0.32 °C) and the SSP5-8.5 scenario will experience the highest temperatures in August with an increase to 3.93 °C. For future maximum temperatures, the SSP1-2.6 scenario would experience lower temperatures in January and the highest in September for the SSP5-8.5 scenario.

Under the SSP scenarios, precipitation increased approximately by 3.42% for the SSP1-2.6 scenario, 6.24% for the SSP2-4.5 scenario, 6.81% for the SSP3-7.0 scenario and 5.52% for the SSP5-8.5 scenario. Average yearly minimum and maximum temperatures increased between 1-4°C across all scenarios (Fig. 2). Details of the statistical analysis of the historical (1980–2023) and future SSP scenarios (2024–2100) for precipitation, maximum temperature and minimum temperature include the mean, median, coefficient of variance (%), range, kurtosis, skewness and percentage change are shown in Supplemental Data Table S2.

Month	Historical precipitation (mm)	SSP1-2.6 (mm)	SSP 2-4.5 (mm)	SSP 3–7.0 (mm)	SSP 5-8.5 (mm)
Jan	1.09	1.02	1.10	1.21	1.23
Feb	1.56	1.74	1.73	2.07	2.14
Mar	2.00	2.29	2.29	2.62	2.55
Apr	2.80	3.11	3.73	3.40	3.43
May	3.04	3.49	3.81	4.19	4.20
Jun	5.59	4.36	4.74	5.48	4.64
Jul	9.90	9.84	10.35	9.93	10.10
Aug	9.80	10.75	10.12	9.41	9.27
Sep	4.94	5.42	5.75	5.56	5.66
Oct	1.79	1.81	1.74	1.93	1.87
Nov	1.76	1.87	1.73	1.68	1.72
Dec	1.12	1.32	1.20	1.07	1.18
Month	**Historical Max temperature (°C)**	**SSP1-2.6 (°C)**	**SSP 2-4.5 (°C)**	**SSP 3-7.0 (°C)**	**SSP 5-8.5 (°C)**
Jan	5.42	6.26	7.31	8.47	8.73
Feb	7.91	9.17	9.84	10.98	11.52
Mar	13.52	14.42	15.20	16.18	16.46
Apr	19.80	20.33	20.84	21.72	22.20
May	24.62	25.69	26.14	27.02	27.47
Jun	27.81	29.27	29.80	30.61	31.21
Jul	29.85	32.06	32.84	33.53	34.25
Aug	30.80	33.11	33.94	34.82	35.25
Sep	27.01	29.36	30.10	31.01	31.75
Oct	21.76	23.52	24.26	24.95	25.76
Nov	14.88	16.91	17.55	17.97	18.82
Dec	7.85	9.20	9.78	10.58	11.0
Month	**Historical Min temperature (°C)**	**SSP1-2.6 (°C)**	**SSP 2-4.5 (°C)**	**SSP 3-7.0 (°C)**	**SSP 5-8.5 (°C)**
Jan	−3.03	−3.00	−2.12	−0.95	−0.76
Feb	−1.73	−1.30	−0.87	0.28	0.81
Mar	2.44	2.12	2.80	3.89	4.19
Apr	7.80	7.53	8.09	9.01	9.44
May	13.26	13.15	13.78	14.78	15.17
Jun	18.50	18.90	19.64	20.50	20.85
Jul	22.70	24.33	25.21	25.95	26.34
Aug	23.02	24.98	25.74	26.50	26.95
Sep	18.00	19.47	20.22	21.17	21.77
Oct	11.11	11.29	12.04	12.90	13.56
Nov	4.89	5.64	6.23	6.65	7.52
Dec	−0.90	−0.41	−0.09	0.69	1.13

Table 1. Monthly average precipitation (mm), maximum temperature (°C) and minimum temperature (°C) for historical (1980–2023) and future projections (2024–2100).

Baseline scenario flood risk assessment

The spatial distribution of the baseline scenario for the four indices well represented the flood risk in the YRB (Fig. 3). Flood duration across YRB sub-basins well-represented flooding days in the baseline scenario, with longer flood days in and around sub-basins with dams and urban areas, and 1.14–0.37 recurrence days for some sub-basins. Flood exceedance probability and magnitude showed higher flood probability (0.50) and relative magnitude (27.67) for sub-basins with dams and within urban areas, whereas forested areas had lower probabilities (0.11) and magnitudes (0.37). Flood frequency was higher in dam outlet sub-basins and the basin outlet at 1.10 days per year, and lowest in some sub-basins at 0.40 days per water year. The SWAT model captured the four indices showing consistency with a few sub-basins and inconsistency with most other sub-basins. Flood duration and magnitude show similar flood risk patterns, and flood exceedance and frequency also show a similar flood pattern in the baseline scenario for the 2-year flood recurrence threshold, thus capturing the flooding in the various sub-basins.

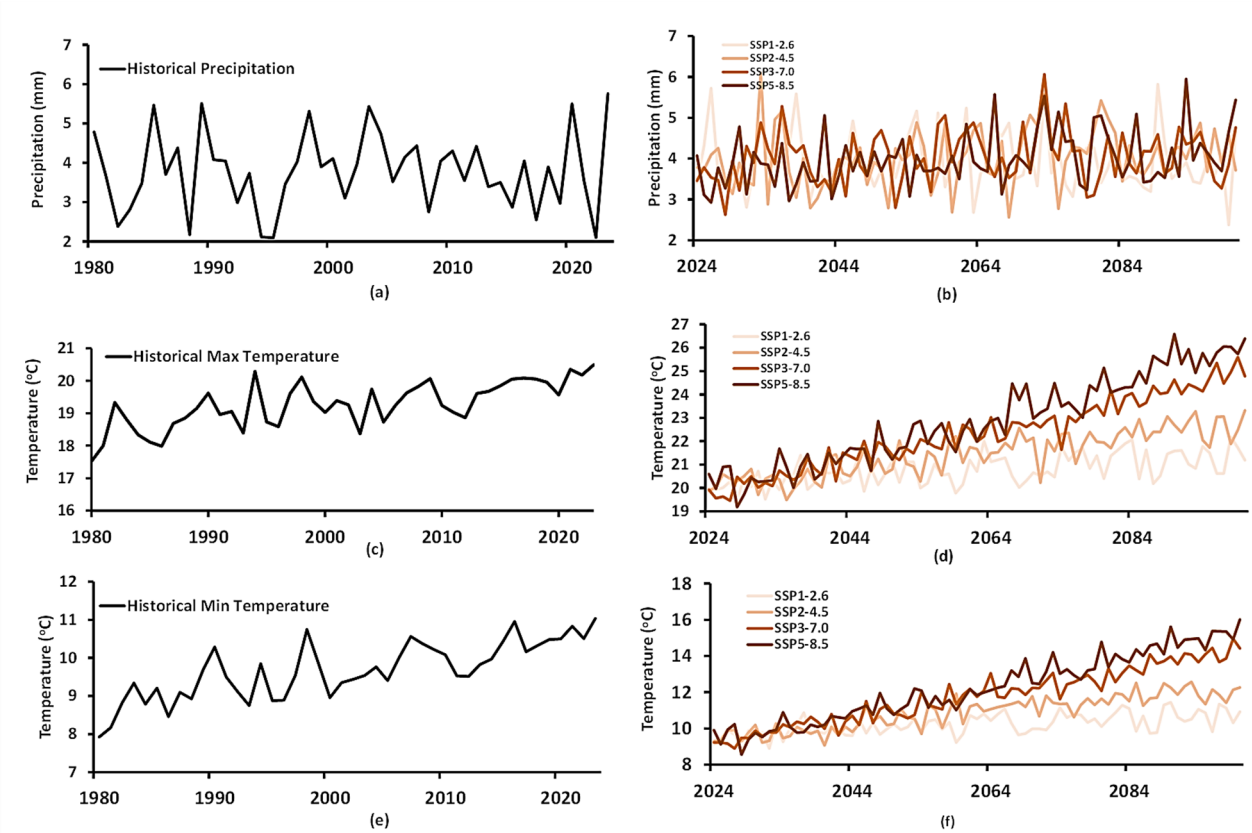

Fig. 2. Average yearly precipitation, maximum temperature and minimum temperature (**a**) Historical precipitation (**b**) Combined SSPs precipitation (**c**) Historical maximum temperature (**d**) Combined SSPs maximum temperature (**e**) Historical minimum temperature (**f**) Combined SSPs minimum temperature.

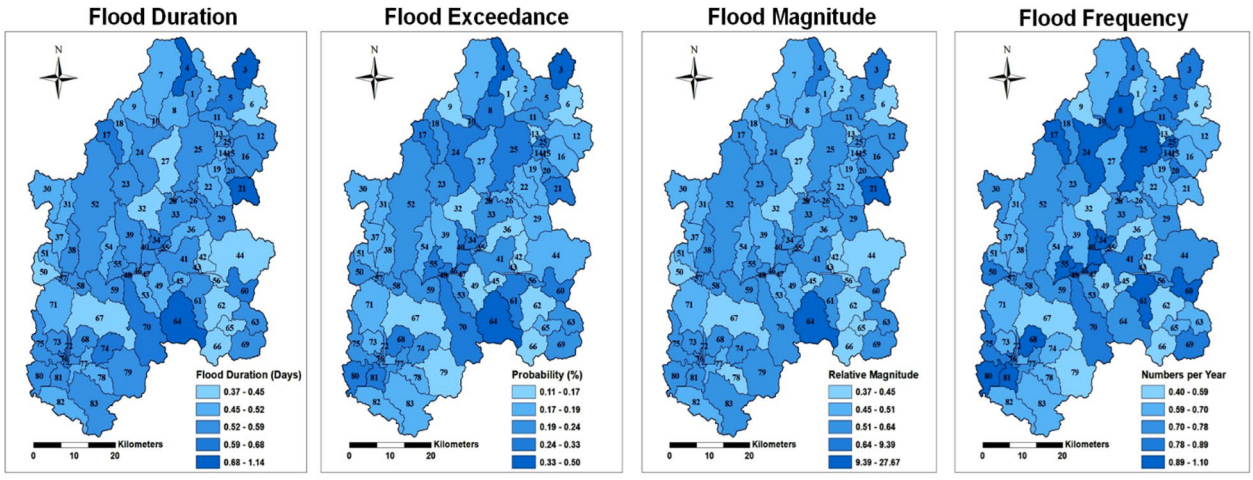

Fig. 3. Spatial distribution of flood risk for the baseline scenario from 1980 to 2023.

Climate model flood risk assessment

The spatial distribution of climate change results indicated future flood risk across sub-basins to the baseline scenario under SSP scenarios for a 2-year return period in the range of no risk–high risk. In the SSP1-2.6 mid-century scenario, spatial distributions of flood indices ranged between −35 and 30% across YRB sub-basins. Flood duration and exceedance probability increased by +15% in some sub-basins and decreased in others by -5% from the baseline scenario. Flood magnitude could increase up to 25% in some sub-basins, whereas

it decreased by -35% in others from the baseline scenario. Similar to flood magnitude, flood frequency could increase up to 30% in some sub-basins from the baseline scenario and decrease by -30% in other sub-basins is depicted in (Fig. 4a).

In the SSP1-2.6 end-century scenarios in (Fig. 4b), flood duration and flood magnitude showed an increase up to 20% and decrease up to -30% in sub-basins compared with the baseline scenario. Flood exceedance ranged between − 10% and + 15% and flood frequency between − 55% and 50% among the sub-basins. The number of flood frequencies per year in sub-basins showed a 50% chance of flooding or not flooding with relatively average flood magnitude. Flood duration days were longer in some sub-basins and shorter in others with relatively low flood exceedance probability. Sub-basins with higher flood risk indices are more prone at the dam and reservoir outlets as there could be possibilities of dam breakage or overflow.

Figure 5a indicates the spatial distribution of the four indices for the SSP2-4.5 mid-century scenario from the baseline scenario, with a slight decrease (-5%) and increase (20%) observed in flood duration, indicating low flood risk in the YRB. Flood exceedance decreased by -5% in some sub-basins and increased to 45% of the baseline scenario. Flood magnitude decreased by -15% in some sub-basins and increased by 35% in others from the baseline scenario. Flood frequency increased by 30% and decreased by -15% across the YRB sub-basins. The number of flood-duration days shows a low flood risk for the SSP2-4.5 mid-century and moderate flood risk for flood exceedance. The number of flood frequencies indicates no flood occurrence in some sub-basins and moderate flood risk in other sub-basins with a relatively low flood magnitude in the YRB.

The SSP2-4.5 end-century scenario showed results similar to those of the SSP2-4.5 mid-century scenario from the baseline scenario, with slight increases in some sub-basins for the four flood indices. The spatial pattern of flood duration showed an increase up to 20% and a decrease of -5%. Flood exceedance probability increased by 45% and decreased up to -5%. Flood magnitude ranged between − 5% and 35%, and flood frequency from − 20 to 30% across the sub-basins. Figure 5b shows that a few sub-basins would experience low flood frequency, whereas a major basin showed a slight increase in flood risk. A few sub-basins show a low flood frequency whereas a major indicates a slight increase in flood risk in the YRB. The number of flood days indicates on

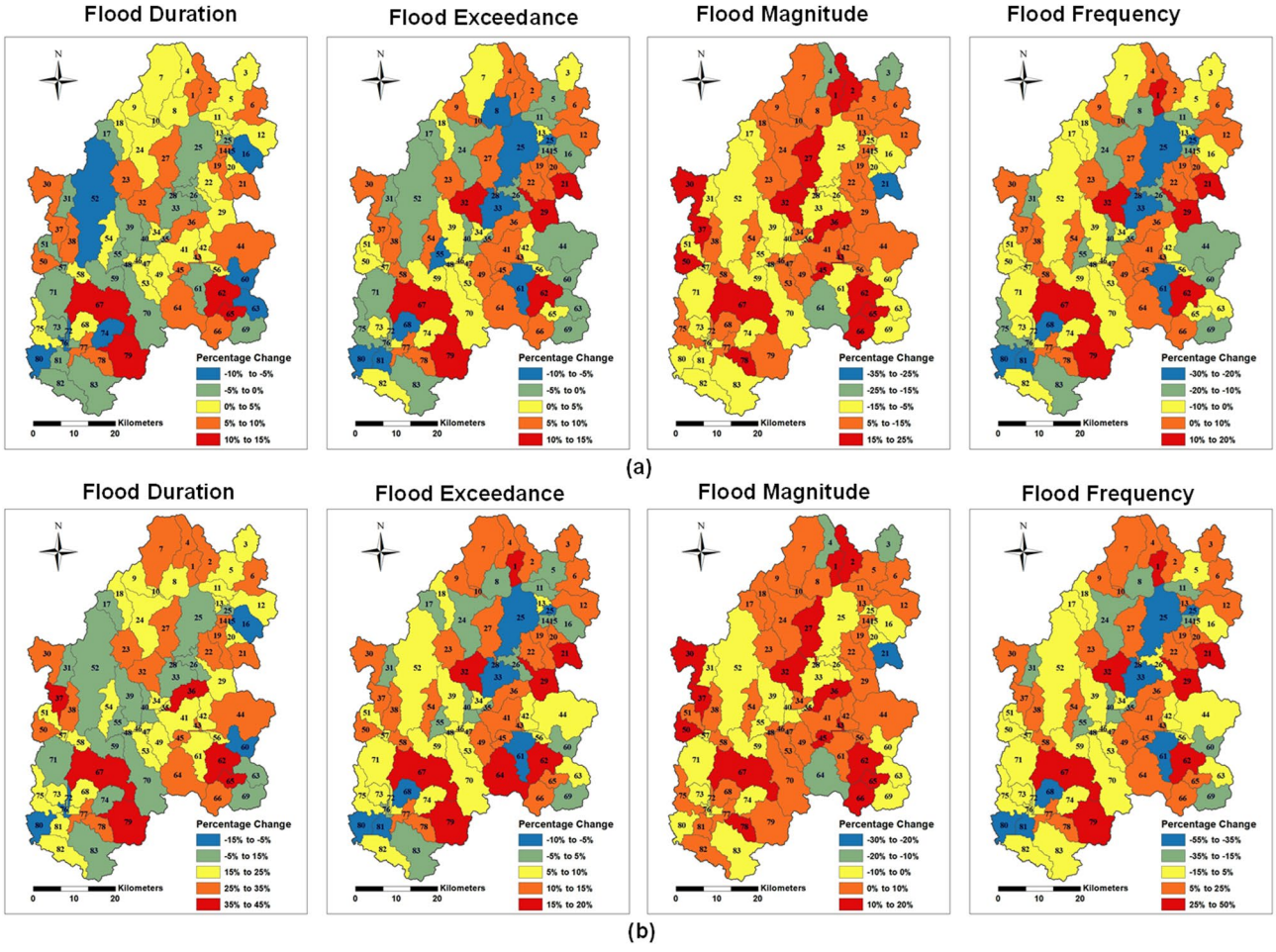

Fig. 4. Percentage change between baseline and mid-century SSP1-2.6 scenario (**a**) mid-century scenario and (**b**) end-century scenario. Flood frequency of the end scenario shows the most significant changes, with some sub-basins showing little or no flood risk with − 55%, while other sub-basins indicate a 50% chance of flood risk.

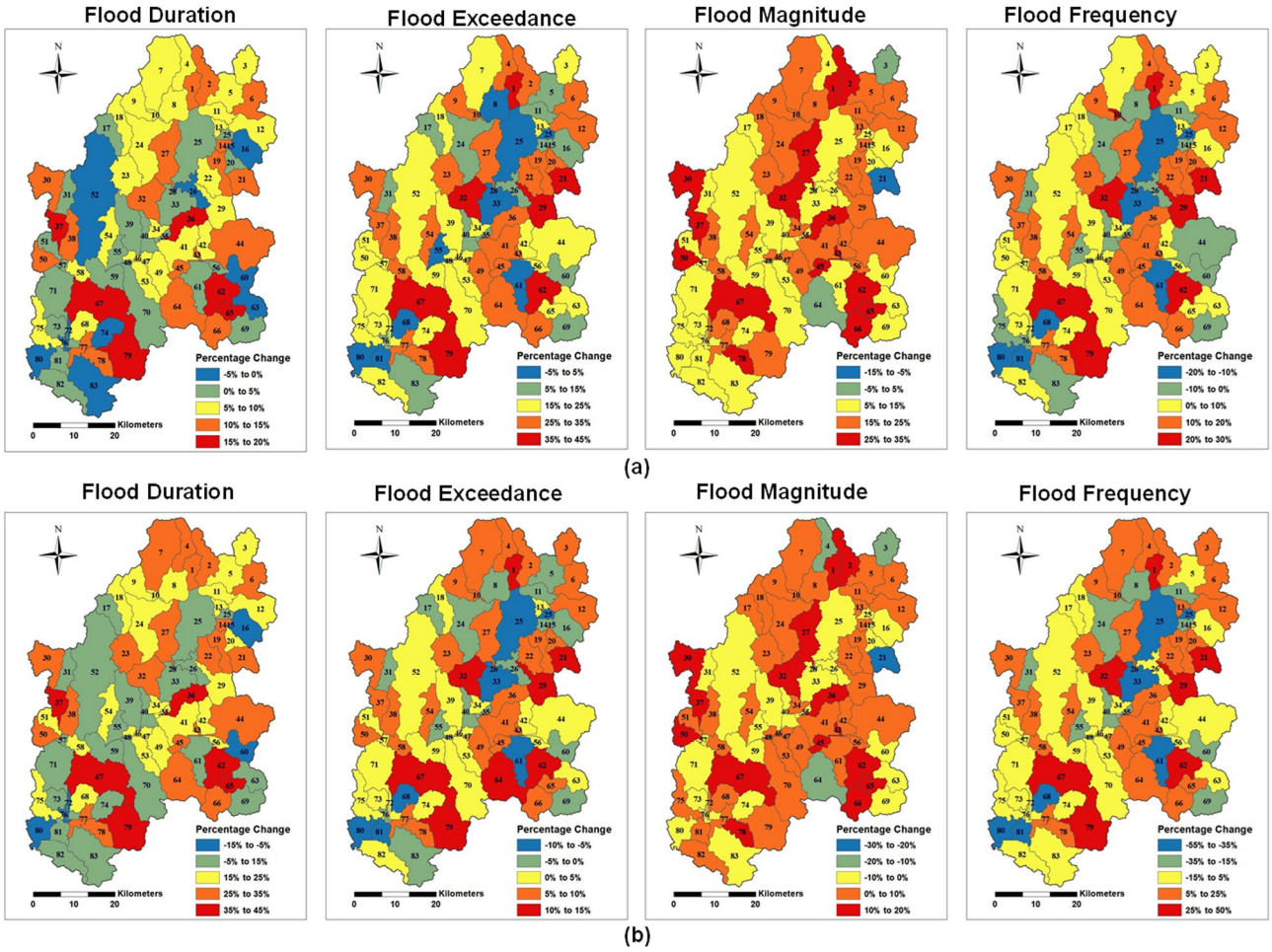

Fig. 5. Percentage change between baseline and mid-century SSP2-4.5 scenario (**a**) mid-century scenario and (**b**) end-century scenario. Flood frequency of the end scenario shows the most significant changes, with some sub-basins showing little or no flood risk with − 55%, while other sub-basins indicate a 50% chance of flood risk.

average a low flood risk in the YRB. Flood exceedance probability shows a moderate flood risk, indicating a higher flood risk magnitude and slight flood frequency in the sub-basins.

Results from the SSP3-7.0 mid-century scenario showed an increase of up to + 25% in the spatial pattern of flood duration, with no decrease among the sub-basins from the baseline scenario. The spatial pattern showed a flood exceedance probability range of -5–45%, a flood magnitude of -10–40%, and a flood frequency between − 10% and 40% in the sub-basins from the baseline scenario. Spatial patterns of flood exceedance probability, magnitude, and frequency indicated moderate flood risk up to 40–45% and, therefore, provable future flood risk. No flood days were predicted in the SSP3-7.0 mid-century in the YRB. Spatial patterns show flood exceedance probability, magnitude, and frequency show a moderate flood risk of up to 40–45%, thus, possible future flood risk (Fig. 6a).

The results of the SSP3-7.0 end-century scenario for all four indices showed an increase across the YRB from the baseline scenario (Fig. 6b). Flood duration and magnitude ranged from − 10 to 40%, flood exceedance probability between − 5 and 25%, and flood frequency between − 40% and 60%. The number of flood days indicated medium flood risk, with most sub-basins showing longer flood days and a few no flood days. Flood exceedance indicated a slight flood risk, and flood magnitude indicated a higher future risk across the sub-basins. The number of flood frequencies indicated a high future flood risk, with some sub-basins increasing up to 60% and other basins as low as -40%.

Figure 7a shows the spatial patterns of flood risk indices for the SSP5-8.5 mid-century scenario from the baseline scenario. Flood duration and exceedance probability showed high flood risk, with increases up to 25% for flood duration days and exceedance probability of approximately 50% in all sub-basins. Flood magnitude ranged between − 5% and 45%, and flood frequency was between − 25% and 25% per year. The number of flood days indicated a longer flood duration, with a probability of medium flood risk in the future. Flood exceedance indicated that the likelihood of flooding could reach 50%. The four indices show a slight flood risk for flood duration and exceedance, whereas flood magnitude and frequency with a higher flood risk in the YRB.

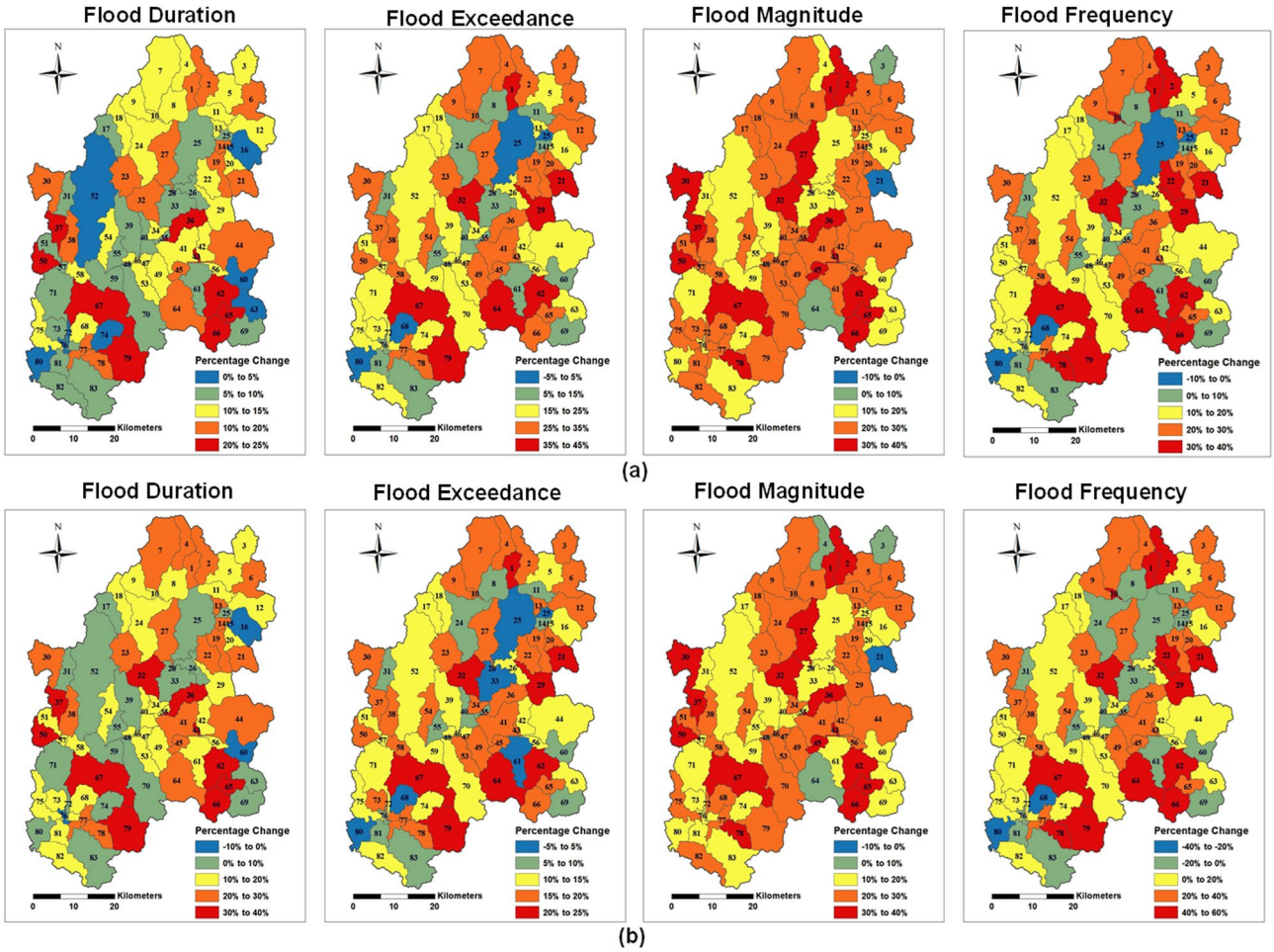

Fig. 6. Percentage change between baseline and mid-century SSP3-7.0 scenario (**a**) mid-century scenario and (**b**) end-century scenario. Flood frequency of the end scenario shows the most significant changes, with some sub-basins showing little or no flood risk with −40%, while other sub-basins indicate a 60% chance of flood risk.

The spatial patterns of the four flood indices for the end-century scenario of SSP5-8.5 showed an average higher flood risk in the YRB than in the baseline scenario. Flood duration increased between 5% and 30% in all sub-basins. Flood exceedance probability ranged from −5 to 25%, magnitude between −5% and 45%, and frequency from −45 to 65%. The four indices showed slight flood risk for flood duration and exceedance, whereas flood magnitude and frequency showed higher flood risk as represented in (Fig. 7b).

Discussion

The SWAT model was developed for the YRB for the baseline scenario (1985–2021) and future climate change scenarios, namely mid-century (2030–2060) and end-century (2070–2100). The model was calibrated (2006–2013) and validated (2014–2021) for the YRB at four weather stations (S1, S2, S3, and S4) with streamflow data at a daily time step. The model's overall performance was satisfactory according to the criteria suggested by Moriasi et al.[51]. Calibrating a model at multiple locations increased the accuracy of the SWAT model and provided a good representation of the watershed[52–54].

Monthly precipitation and temperature trends across the SSPs suggest slight increases in precipitation during the summer monsoon season with higher minimum and maximum temperatures which may result in high water evaporation, possible future droughts, agricultural productivity reduction and possible water scarcity[5]. Results in the study conform with a report in 2009 from the National Institute of Meteorological Research which predicted that future yearly averages for minimum and maximum temperatures would increase by 4 ^{o}C[55]. Temperature and precipitation changes will have a direct impact on flood indices since rising temperatures will raise the frequency of floods by increasing atmospheric moisture and severe precipitation occurrences. Flood occurrences might last longer when there is prolonged, heavy rainfall because it can saturate soils and overwhelm drainage systems[56]. High levels of precipitation and quick melting increase the size of floods by allowing more water to enter river systems in shorter amounts of time and raising peak discharge. Additionally, climate change modifies the statistical distribution of extreme weather occurrences, increasing the likelihood that precipitation would be above historical thresholds and, consequently, the likelihood of flood exceedance[57].

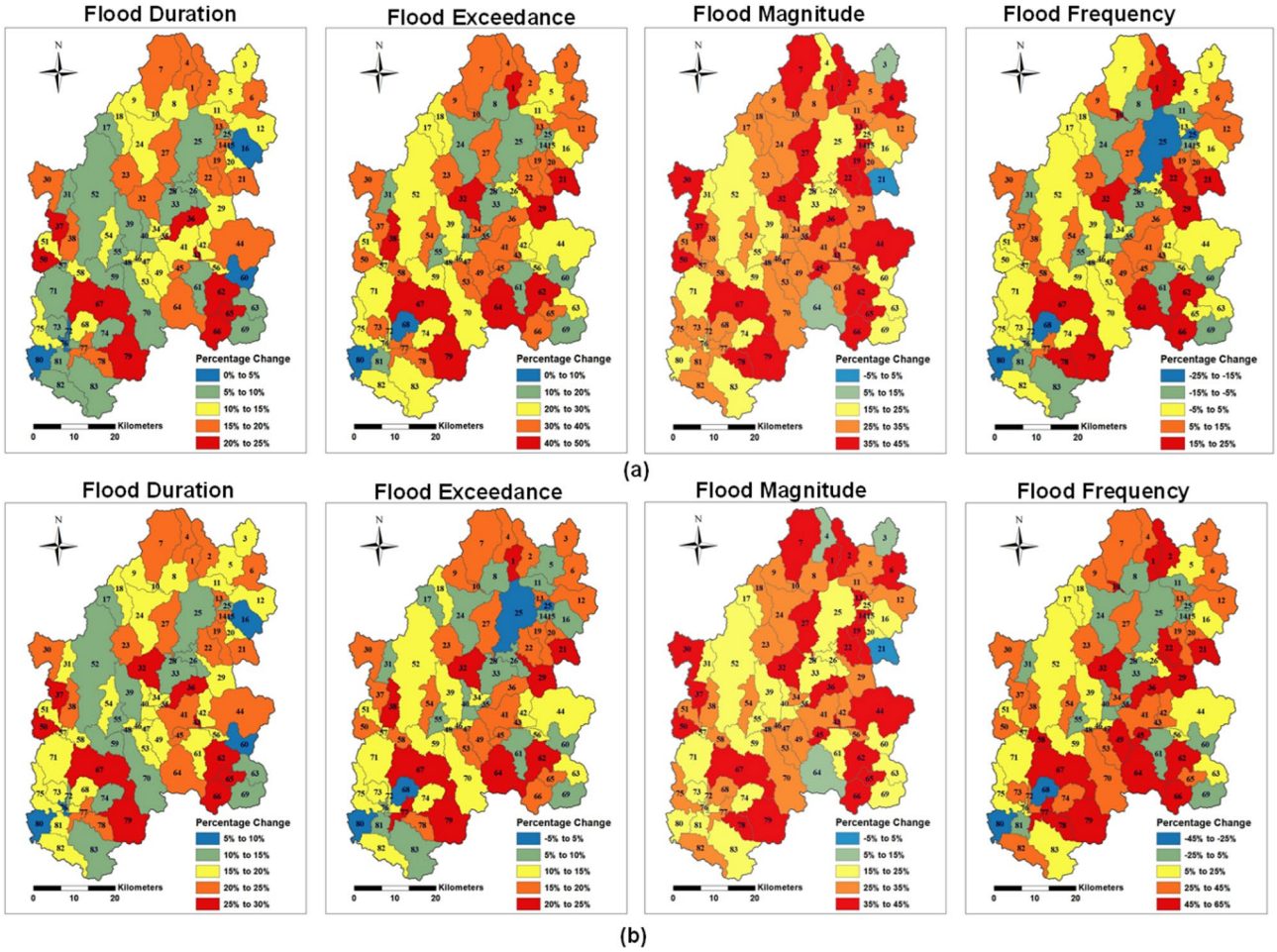

Fig. 7. Percentage change between baseline and mid-century SSP5-8.5 scenario (**a**) mid-century scenario and (**b**) end-century scenario. Flood frequency of the end scenario shows the most significant changes, with some sub-basins showing little or no flood risk with −45%, while other sub-basins indicate a 65% chance of flood risk.

Flood risk assessment for the baseline scenario showed variability in flood effects across different sub-basins, aligning with past and recent flood events in South Korea, where the frequency of disruptive floods has increased over the last decade[5]. In the baseline scenario, some sub-basins experienced lower flood risk characterized by shorter flood durations, lower exceedance probabilities, lower flood magnitudes, and less frequent flood events. These areas are covered predominantly by agricultural land and forests, which likely contribute to their reduced flood vulnerability. Vegetation plays an important role in the reduction of peak flow, and watersheds with vegetation reduce surface runoff, whereas watersheds with little or no vegetation increase runoff[18,22,58,59]. In contrast, other sub-basins exhibited higher flood risk with longer flood durations, higher exceedance probabilities, and more frequent and intense flood events. High risk was found primarily in urbanized areas, where land use patterns and infrastructural development contribute to the increased vulnerability to flooding, confirming the significant effect of urbanization on flood risk[60]. Furthermore, the high flood risk might be due to the presence of dams and reservoirs, as paddy rice farming is the main crop cultivated, and agriculture comprises about 50% of the YRB. With the large dams being constructed in the 70s, an increase in moderate or large rainfall events could lead to dam overtopping and failure, resulting in catastrophic downstream flooding[61,62].

Future flood risks are projected to vary significantly across different SSP (SSP1-2.6, SSP2-4.5, SSP3-7.0 and SSP5-8.5) scenarios, reflecting both the anticipated socioeconomic changes and varying levels of radiative forcing by 2100. In the mid-century SSP1-2.6 scenario, flood durations are projected to decrease by approximately 10%. This reduction suggests that floods could become shorter but potentially more intense, as storm systems could release substantial amounts of rainfall over brief periods[63]. These could overwhelm the drainage systems, causing sudden infrastructure failures, traffic paralysis, and high casualty risks, thus increasing flood vulnerability[64]. On the other hand, in the end-century SSP3-7.0 scenario, flood durations could increase by as much as 40%. This increase indicated the likelihood of prolonged rainfall, resulting in longer-lasting floods that significantly increase the risks of exposure and damage. The shifts in flood duration reflect the complex interplay between changing rainfall patterns and the ability of the landscape to absorb water under warming climate conditions[65,66].

Prolonged flood durations exacerbate infrastructure damage, economic disruption, and public health risks, leading to deeper and longer-term vulnerability that affects both urban and rural areas[67].

Flood exceedance probability, a measure of floods, also changed under different SSP scenarios for a 2-year return period. In the most optimistic SSP1-2.6 scenario, a decrease of 10% in flood exceedance probability was forecast for the mid- and end-century scenarios. Although fewer flood events could occur, the possibility of larger sporadic floods remains, with a higher likelihood that water levels surpass critical thresholds in the drainage system. In stark contrast, the end-century SSP5-8.5 scenario predicted a 50% increase in exceedance probability, driven by more intense storms, more substantial precipitation, and possibly reduced land absorption capacity owing to urbanization and deforestation[68]. Higher flood exceedance probability leads to chronic flood exposure, accelerating infrastructure degradation and deepening regional vulnerability, particularly in urban and low-adaptive-capacity[69].

Flood magnitude is expected to vary, with a 35% reduction in the mid-century scenario under SSP1-2.6 and a 45% increase under SSP5-8.5 for mid- and end-century scenarios. The decrease in flood magnitude in SSP1-2.6 suggested lower peak discharges, probably because of less intense precipitation patterns. However, the projected increase in flood magnitude under SSP5-8.5 signaled more severe flood events caused by intense and prolonged rainfall. These results are consistent with several studies that indicate an increase in flood magnitude in South and East Asia[70]. However, the magnitude of extreme rainfall events is expected to increase along with higher temperatures[71]. These can be characterized by greater flow volumes and water depths, increasing flood vulnerability, leading to greater economic and human losses, especially in densely populated and low-lying areas[72].

Flood frequency, closely tied to storm intensity and recurrence, is projected to decrease by 55% for the end-century SSP1-2.6 scenario, indicating fewer flood events because of less frequent or intense storms. Conversely, SSP5-8.5 forecasts a 65% increase in flood frequency by mid-century, suggesting more regular and intense storm events, particularly in urban and rural areas. Rising flood occurrence of flood events reduces the recovery time between flood incidents and compounding socio-economic impacts that strain infrastructure, overwhelm emergency services, and disrupt livelihoods[72].

Spatial and temporal distributions of rainfall and large-scale climate indices affect the magnitude and frequency of high flows[73]. Based on this study's projections for the mid- and end-century periods, most sub-basins in the YRB have a higher flood risk. These findings are similar to those of a study conducted by Kim et al.[17]indicating that the YRB has the highest flood risk in South Korea. Future flood risk and vulnerability will be multi-dimensional, driven by the combined effects of increased flood magnitude, duration, frequency, and exceedance probability. These changes are not uniformly distributed, indicating the need for adaptation plans in the YRB. Integrating these flood indices into planning frameworks allows for a more nuanced understanding of both acute and chronic flood threats. Policymakers and urban planners should prioritize sub-basins with high exceedance probability and limited recovery capacity, while strengthening infrastructure and early warning systems in the sub-basins exposed to frequent or severe flood events.

A limitation of this study is the simulation of land use/cover changes, which are driven by urbanization, deforestation, and agricultural expansion. Since the SWAT model assumes a stationary LULC, it may underestimate future flood risks, as changes in infiltration, surface runoff, and channel flow significantly impact flood frequency and magnitude. Integrating non-stationary LULC scenarios and using projected landcover maps coupled with GCMs could enhance the accuracy of flood risk predictions and reduce uncertainty, ensuring effective watershed management planning. Exploring the use of multiple CMIP6 GCMs and RCMs may improve the accuracy and credibility of impact analysis by capturing uncertainty and bracketing possible flood risk outcomes as only 5 RCMs were employed in this study. Future research should further integrate socio-economic and infrastructure data to develop holistic flood risk (hazard, exposure and vulnerability) assessments and adaptive response strategies under changing climate conditions. Also, more extensive analysis integrating future changes in the snowmelt and baseflow regimes should be carried out to offer reliable predictions of the highest potential flood risk.

Methods

SWAT model setup and evaluation

Details of the SWAT model description are shown in Supplementary Note S1 and Supplementary Data Fig. S3. We used the software ArcSWAT 2020 revision 681, employing land use, digital elevation model (DEM), streamflow, dam, and soil data as inputs for model development. The 30 m × 30 m resolution ASTER Global Digital Elevation Model (GDEM) was used to obtain DEM data, the Harmonized World Soil Database (HWSD v121) provided soil data, and the USGS EROS Archive—Land Cover Products—Global Land Cover Characterization (GLCC) map was used for land use data (Supplementary Data Fig. S4). Hydrological response units (HRUs) were defined using thresholds, namely land use 10%, soil 10%, and slope maps 15%. The watershed was divided into 502 HRUs and 83 sub-basins to represent the YRB adequately. Daily weather data for 1980–2021 were obtained from eight weather stations through the Korean Meteorological Administration (KMA) shown on Supplementary Data Table S3. The Soil Conservation Service (SCS) CN method was used to predict surface runoff, and the daily CN was determined as a function of soil moisture. Route channel flow was calculated using the Muskingum method, and potential ET was estimated using the Penman–Monteith technique. Four agricultural dams were simulated as reservoirs in the model (Supplementary Data Fig. S5, S6, S7 and S8). Supplementary Data Table S4 shows the details of reservoir characteristics. The CO_2 concentrations were varied for different scenarios.

Sensitivity and uncertainty analyses were conducted using the SWAT calibration and uncertainty program (SWAT-CUP). Multivariable and multi-site calibration approaches were used in the YRB at daily and monthly time steps for the four hydrological stations. The model was calibrated for 2006–2013, and the 2014–2021 streamflow dataset was validated. Nash–Sutcliffe model efficiency (NSE), r-factor, RMSE-observation standard

deviation ratio (RSR), root mean square error (R^2), p-factor, and percentage bias (PBIAS) were used for model evaluation and validation[51,74–77]. Details of the equations can be seen in the supplementary data equation S1.

Using the generalized likelihood uncertainty estimation approach in SWAT-CUP, the most sensitive factors were identified that directly affected streamflow, namely SOL_AWC, GW_DELAY, CN, CH_K2, and ALPHA_BF (Supplementary Data Table S5). According to the criteria proposed by Moriasi et al.[51], discharge simulations for monthly or daily model statistics in a range NSE > 0.5, RSR ≤ 0.7, and PBIAS < 15%, $R^2 > 0.6$ are regarded as acceptable.

Climate model selection, downscaling, and bias correction

To conduct this study, high-resolution climate change projection data of precipitation and temperature are essential. In South Korea, five CMIP6 regional climate models (RCMs) are used to generate and disseminate high-resolution climate change projection data for the East Asian region, with a horizontal resolution of 25 km. These projections are based on the four SSP scenarios (1-2.6, 2-4.5, 3–7.0, and 5-8.5) defined by the IPCC[78–85].

In this study, future projections of average climate conditions and extreme climate events across six regions of South Korea were made using the new high-resolution (1 km) climate change scenario developed using the PRIDE (PRISM-based Dynamic Downscaling Error Correction) method, which is based on MK-PRISM (Modified Korean-Parameter elevation Regressions on Independent Slopes Model)[84,85] generated through the PRIDE method (PRISM-based Dynamic Downscaling Error Correction)[84]. Using the Barnes objective analysis method, the 25 km resolution East Asia climate change scenario data from five regional climate models (RCMs) in the second phase of the CORDEX-East Asia project were first interpolated to a 1 km resolution for South Korea to align them with the high-resolution gridded observational data[85]. The Hadley Center Global Environmental Model version 3 regional climate model (HadGEM3-RA), Weather Research and Forecasting (WRF), Consortium for Small-scale Modeling (COSMO)-Climate Limited-area Modeling (CLM) (CCLM), Regional Climate Model version 4.0 (RegCM), and Global/Regional Integrated Model system (GRIMs) were the five RCMs that were used. These models are described in detail in Kim et al.[84]. After that, the daily seasonal cycles from the regional climate models were substituted with those from the gridded observational data in the interpolated 1 km data. With the response to climate change forcings preserved, this stage eliminated the systematic bias in the climate models' seasonal cycles, producing the final high-resolution climate change scenario. To learn more about this approach and validation, see Kim & Kim[85] and Kim et al.[84]. Using the Quantile Delta Mapping (QDM) technique, which was suggested by Cannon et al.[86], an extra bias correction was included since precipitation shows comparatively substantial systematic biases in climate models.

Using four SSP scenarios and five model ensemble members, the final high-resolution climate change scenarios were created for a total of 80 years (2021–2100). For six administratively divided areas of South Korea, future changes in the average climate and extreme climatic events were projected using the high-resolution (1 km) climate change scenarios produced by the approach presented. More precise forecasts at the levels of over 220 cities, counties, and districts, 17 metropolitan and provincial regions, and roughly 3,500 towns, townships, and neighborhoods will be provided by future research. In terms of temperature and precipitation, the expected changes in the average climate were compared between the current period (1979–2014) and two future periods: the mid-century (2030–2060) and the end-century (2070–2100). Both individual ensemble members and the ensemble mean from the five-model ensemble were projected into the future. More information on the RCMs and the SSPs is detailed in Supplementary Data Tables S6 and S7.

Flood indices

To evaluate future flood risk in the YRB, four indices (exceedance probability, duration, magnitude, and frequency) were calculated using the simulated daily flow rate for each of the 83 sub-basins in the SWAT model. Flood events were identified using a 2-year return period threshold for each sub-basin, derived from baseline climate simulations. Annual maximum daily flows were extracted and fitted with a Log-Pearson Type III distribution using the method of moments based on log-transformed data. The 2-year flood threshold, representing a 50% annual exceedance probability, was calculated by adjusting the standard normal variate for skewness and back-transforming to the original scale. This consistent threshold was applied across all scenarios to identify flood events and compute flood indices. For future scenarios, this threshold was derived from present climate simulations. Details of the flood indices are explained below.

Flood exceedance probability (FEP) is the probability of a flood event of a certain magnitude equaling or exceeding each year. The FED index represents the proportion of days in a given water year (June–September) where the simulated flow is greater than or equal to the index. This index is used to compute the likelihood of daily flow above the index. The percentage is averaged over the simulation period Eq. (1).

$$FEDI = \sum_{i=1}^{n} \frac{FED}{N} \times 100\% \tag{1}$$

where FED is the flood exceedance probability of water year *i*; N is the total number of years in simulation years; *n* is the number of days when a flood occurs in a water year *i*; *FEDI* represents the average flood exceedance probability for a sub-basin.

Flood duration (FD) is the number of consecutive days of flooding in a flood event. The FD index was computed as the total amount of time during which the water level surpassed the threshold indices in a water year. The flood duration index is computed using the average for all years Eq. (2).

$$FDI = \frac{\sum_{i=1}^{n} D_i}{N} \tag{2}$$

where D_i is the number of days flood events occur in a water year i; n is the total number of flood occurrences in a water year i; N is the total number of years in the simulation years; FDI represents the average flood duration index for each sub-basin.

The flood magnitude index indicates the proportional size of floods relative to the flood indices. The average daily discharge is calculated for each flood occurrence Eq. (3).

$$FMI = \frac{Q_{peak}}{Q_{threshold}} \tag{3}$$

where Q_{peak} is the peak discharge in a water year *i*; $Q_{threshold}$ is the threshold value of the return period; *FMI* is the flood magnitude index for each sub-basin at a given threshold.

Flood frequency (FF) quantifies the frequency of flood events exceeding the flood indices in a water year. The FF index is calculated as the average discharge of flood events in a water year Eq. (4).

$$FFI = \frac{N_{flood}}{N} \tag{4}$$

where N_{flood} is the number of flood occurrences in a water year i; N is the total number of years in the simulation years; *FFI* is the average flood frequency index for a sub-basin.

Flood indices were calculated for each model in the climate model ensemble under future conditions (2030–2060 and 2070–2100) and historical conditions (1980–2021) using 2-year flood recurrence thresholds. To determine whether the flood risk of each sub-basin increased or decreased under the influence of future climatic circumstances, the findings are provided as a percentage of change in the flood indices between the baseline and future scenarios.

Data availability

All the datasets utilized for the study this study are publicly available which compromises of the ASTER Global Digital Elevation Model data can be accessed from https://earthexplorer.usgs.gov/; Harmonized World Soil Data base v1.21 data from https://www.fao.org/soils-portal/data-hub/soil-maps-and-databases/harmonized-world-soil-database-v12; USGS EROS Archive - Land Cover Products - Global Land Cover Characterization (GLCC) data from https://www.usgs.gov/centers/eros/science/usgs-eros-archive-land-cover-products-global-land-cover-characterization-glcc; Korean meteorological data from https://data.kma.go.kr/; streamflow, dam inflow and outflow data from http://www.wamis.go.kr/; and the shared socioeconomic pathways climate change data from http://www.climate.go.kr/. The data supporting the findings of this study are available from the first author, [Agbortoko Bate Ashu], upon reasonable request.

Code availability

The code to determine four flood indices using the Soil and Water Assessment Tool, MATLAB-scripts and R-scripts are publicly available and can be accessed https://github.com/yuchenw/Flood-Index.

Received: 17 December 2024; Accepted: 14 July 2025
Published online: 18 July 2025

References

1. Nam, W. H., Kim, T., Hong, E. M. & Choi, J. Y. Regional climate change impacts on irrigation vulnerable season shifts in agricultural water availability for South Korea. *Water* **9**, 735. https://doi.org/10.3390/w9100735 (2017).
2. Chen, J., Chen, W. & Huang, G. Assessing urban pluvial flood resilience based on a novel grid-based quantification method that considers human risk perceptions. *J. Hydrol.* **601**, 126601. https://doi.org/10.1016/j.jhydrol.2021.126601 (2021).
3. Chen, M., Papadikis, K. & Jun, C. An investigation on the non-stationarity of flood frequency across the UK. *J. Hydrol.* **597**, 126309. https://doi.org/10.1016/j.jhydrol.2021.126309 (2021).
4. Ministry of Land. *Infrastructure and Transport. Nation-Wide River Basins Investigation Report* (MOLIT, 2012).
5. Ashu, A. B. & Lee, S. I. Assessing climate change effects on water balance in a monsoon watershed. *Water* **12**, 2564. https://doi.org/10.3390/w12092564 (2020).
6. Ministry of Land. Infrastructure and Transport. *The 4th Long-Term Comprehensive Plan of water Resources*. (MOLIT, 2016).
7. Wang, W. J. et al. Flood risk assessment of the Naeseongcheon stream basin, Korea using the grid-based flood risk index. *J. Hydrol. Reg. Stud.* **51**, 101619. https://doi.org/10.1016/j.ejrh.2023.101619 (2024).
8. Kim, J., Park, J., Park, S. & Kang, J. Enhancing water management and urban flood resilience using hazard capacity factor design (HCFD) model: case study of Eco-Delta city, Busan. *Sustain. Cities Soc.* **115** https://doi.org/10.1016/j.scs.2024.105851 (2024).
9. Salman, A. M. & Li, Y. Flood risk assessment, future trend modeling, and risk communication: A review of ongoing research. *Nat. Hazards Rev.* **19**, 04018011. https://doi.org/10.1061/(ASCE)NH.1527-6996.0000294 (2018).
10. Vojtek, M. & Vojteková, J. Flood hazard and flood risk assessment at the local Spatial scale: A case study. *Geom. Nat. Hazards Risk.* **7**, 1973–1992. https://doi.org/10.1080/19475705.2016.1166874 (2016).
11. Kwak, J. et al. Evaluation of future flood probability in agricultural reservoir watersheds using an integrated flood simulation system. *J. Hydrol.* **628**, 130463. https://doi.org/10.1016/j.jhydrol.2023.130463 (2024).
12. Hirabayashi, Y. et al. Global flood risk under climate change. *Nat. Clim. Change.* **3**, 816–821. https://doi.org/10.1038/nclimate1911 (2013).
13. Salas, J. D. & Obeysekera, J. Probability distribution and risk of the first occurrence of k extreme hydrologic events. *J. Hydrol. Eng.* **24**, 1–10. https://doi.org/10.1061/(ASCE)HE.1943-5584.0001809 (2019).
14. Hecht, J. S. & Vogel, R. M. Updating urban design floods for changes in central tendency and variability using regression. *Adv. Water Resour.* **136**, 103484. https://doi.org/10.1016/j.advwatres.2019.103484 (2020).
15. Tabari, H. Climate change impact on flood and extreme precipitation increases with water availability. *Sci. Rep.* **10**, 13768. https://doi.org/10.1038/s41598-020-70816-2 (2020).

16. Slater, L. et al. Global changes in 20-year, 50-year, and 100-year river floods. *Geophys. Res. Lett.* **48** https://doi.org/10.1029/2020GL091824 (2021).
17. Kim, S. et al. Increasing extreme flood risk under future climate change scenarios in South Korea. *Weather Clim. Extremes*. **39**, 100552. https://doi.org/10.1016/j.wace.2023.100552 (2023).
18. Yang, S. & Cui, X. Building regional sustainable development scenarios with the SSP framework. *Sustainability* **11**, 5712. https://doi.org/10.3390/su11205712 (2019).
19. Moss, R. H. et al. The next generation of scenarios for climate change research and assessment. *Nature* **463**, 747–756 https://doi.org/10.1038/nature08823 (2010).
20. van Vuuren, D. P. et al. Arnell, N. A proposal for a new scenario framework to support research and assessment in different climate research communities. *Glob Environ. Change*. **22**, 21–35. https://doi.org/10.1016/j.gloenvcha.2011.08.002 (2012).
21. O'Neill, B. C. et al. The roads ahead: narratives for shared socioeconomic pathways describing world futures in the 21st century. *Glob Environ. Change*. **42**, 169–180. https://doi.org/10.1016/j.gloenvcha.2015.01.004 (2017).
22. Zhang, Y., Wang, Y., Chen, Y., Liang, F. & Liu, H. Assessment of future flash flood inundations in coastal regions under climate change scenarios – A case study of Hadahe river basin in Northeastern China. *Sci. Total Environ.* **693**, 133550. https://doi.org/10.1016/j.scitotenv.2019.07.356 (2019).
23. Adeyi, Q. et al. Developing a hydrological model for evaluating the future flood risks in rural areas. *J. Korea Water Resour. Assoc.* **56**, 955–967. https://doi.org/10.3741/JKWRA.2023.56.12.955 (2023).
24. Sunyer, M. A. et al. Inter-comparison of statistical downscaling methods for projection of extreme precipitation in europe, hydrol. *Earth Syst. Sci.* **19**, 1827–1847. https://doi.org/10.5194/hess-19-1827-2015 (2015).
25. Tabari, H., Paz, S. M., Buekenhout, D. & Willems, P. Comparison of statistical downscaling methods for climate change impact analysis on precipitation-driven drought. *Hydrol. Earth Syst. Sci.* **25**, 3493–3517. https://doi.org/10.5194/hess-25-3493-2021 (2021).
26. Onarun, T., Thepprasit, C. & Sittichok, K. Development of statistical downscaling methods for the assessment of rainfall characteristics under climate change scenarios. *J. Water Clim. Chan.* **14** (9), 2970–2987. https://doi.org/10.2166/wcc.2023.490 (2023).
27. De Niel, J., Van Uytven, E. & Willems, P. Uncertainty analysis of climate change impact on river flow extremes based on a large multi-model ensemble. *Water Resour. Manage.* **33**, 4319–4333. https://doi.org/10.1007/s11269-019-02370-0 (2019).
28. Hosseinzadehtalaei, P., Tabari, H. & Willems, P. Climate change impact on short-duration extreme precipitation and intensity–duration–frequency curves over Europe. *J. Hydrol.* **590**, 125249. https://doi.org/10.1016/j.jhydrol.2020.125249 (2020).
29. Chae, S. T. & Chung, E. S. Significant contribution of bias correction methods to uncertainty in future runoff projections under CMIP6 climate change. *J. Hydrol: Reg. Stud.* **56**, 101973. https://doi.org/10.1016/j.ejrh.2024.101973 (2024).
30. Xu, X. et al. Evaluating the impact of climate change on fluvial flood risk in a mixed-use watershed. *Environ. Modell Softw.* **122**, 104031. https://doi.org/10.1016/j.envsoft.2017.07.013 (2019).
31. Han, H., Kim, D. & Kim, H. S. *Inundation Anal. Coastal. Urban Area Under Clim. Change Scenarios Water MDPI*, **14**, 1159–1178, (2022).
32. Xu, K., Zhuang, Y., Bin, L., Wang, C. & Tian, F. Impact assessment of climate change on compound flooding in a coastal City. *J. Hydrol.* **617**, 129166. https://doi.org/10.1016/j.jhydrol.2023.129166 (2023).
33. Arnold, J. G., Srinivasan, R., Muttiah, R. S. & Williams, J. R. Large-area hydrologic modeling and assessment: part I. Model development. *J. Am. Water Resour. Assoc.* **34**, 73–89. https://doi.org/10.1111/j.1752-1688.1998.tb05961.x (1998).
34. Shadmehri Toosi, A., Doulabian, S., Ghasemi Tousi, E., Calbimonte, G. H. & Alaghmand, S. Large-scale flood hazard assessment under climate change: A case study. *Ecol. Eng.* **147**, 105765. https://doi.org/10.1016/j.ecoleng.2020.105765 (2020).
35. Shrestha, S. & Lohpaisankrit, W. Flood hazard assessment under climate change scenarios in the Yang river basin, Thailand. *Int. J. Sustain. Built Environ.* **6**, 285–298. https://doi.org/10.1016/j.ijsbe.2016.09.006 (2017).
36. Berhanu, D. et al. Evaluation of CMIP6 models in simulating seasonal extreme precipitation over Ethiopia. *Weather Clim. Extremes*. **100752** https://doi.org/10.1016/j.wace.2025.100752 (2025).
37. Gupta, R., Prakash, P. & Chembolu, V. Multi criteria evaluation of downscaled CMIP6 models in predicting precipitation extremes. *Atmos. Res.* **315**, 107921. https://doi.org/10.1016/j.atmosres.2025.107921 (2025).
38. Liu, Y. et al. Evaluation and future projection of compound extreme events in China using CMIP6 models. *Clim. Change*. **178** (2), 1–24. https://doi.org/10.1007/s10584-024-03856-6 (2025).
39. Yalcin, E. Assessing future changes in flood frequencies under CMIP6 climate projections using SWAT modeling: A case study of Bitlis creek, Turkey. *J. Water Clim. Change*. **15** (5), 2212–2231 (2024).
40. Do, H. X., Le, T. H., Le, M. H., Nguyen, D. L. T. & Do, N. C. Future changes in Hydro-Climatic extremes across vietnam: evidence from a Semi-Distributed hydrological model forced by downscaled CMIP6 climate data. *Water* **16** (5), 674. https://doi.org/10.3390/w16050674 (2024).
41. Dysarz, T., Marcinkowski, P., Wicher-Dysarz, J., Piniewski, M. & Mirosław-Świątek, D. Kundzewicz,Z.W. Assessment of climate change impact on flood hazard zones. *Water Resour. Manage.* **39**, 963–977. https://doi.org/10.1007/s11269-024-04002-8 (2025).
42. Hwang, J., Ahn, J., Jeong, C. & Heo, J. H. A study on the variation of design flood due to climate change in the ungauged urban catchment. *J. Korea Water Resour. Assoc.* **51**, 395–404 (2018).
43. Lee, T., Kim, J. S. & Chen, J. Spatiotemporal characteristics and hydrological implications of downscaled hourly precipitation climate scenarios for South Korea. *Int. J. Climatol.* **42**, 1253–1266. https://doi.org/10.1002/joc.7300 (2022).
44. Son, K. H., Lee, B. J. & Bae, D. H. Assessment on flood characteristics changes using Multi-GCMs climate scenario. *J. Korea Water Resour. Assoc.* **43**, 789–799. https://doi.org/10.3741/JKWRA.2010.43.9.789 (2010).
45. Kwak, J. et al. Assessment of future flood according to climate change, rainfall distribution and CN. *J. Korean Soc. Agric. Eng.* **62**, 85–95 (2020). (in Korean).
46. Postel, S. & Richter, B. *Rivers for Life: Managing Water for People and Nature* (Island, 2012).
47. Ashu, A. B. & Lee, S. I. Multi-site calibration of hydrological model and spatio-temporal assessment of water balance in a monsoon watershed. *Water* **15**, 360. https://doi.org/10.3390/w15020360 (2023).
48. Lee, K. H., Kang, T. W., Ryu, H. S., Hwang, S. H. & Kim, K. Analysis of Spatiotemporal variation in river water quality using clustering techniques: A case study in the Yeongsan river, Republic of Korea. *Environ. Sci. Pollut Res.* **27**, 29327–29340. https://doi.org/10.1007/s11356-020-09276-0 (2020).
49. Kim, S. et al. Evaluation of agricultural water supply and selection of deficient districts in Yeongsan river basin of South Korea considering supply priority. *Water* **14**, 298. https://doi.org/10.3390/w14030298 (2022).
50. Cheng, C. Spatial climate justice and green infrastructure assessment: A case study for the Huron river watershed, michigan, USA. *GI Forum*. **1**, 176e190 (2016).
51. Moriasi, D. N., Gitau, M. W., Pai, N. & Daqqupati, P. Hydrologic and water quality models: performance measures and evaluation criteria. *Trans. ASABE*. **58**, 1763–1785. https://doi.org/10.13031/trans.58.10715 (2015).
52. Pandey, V. P., Dhaubanjar, S., Bharati, L. & Thapa, B. R. Spatio-temporal distribution of water availability in Karnali-Mohana basin, Western nepal: hydrological model development using multi-site calibration approach (Part-A). *J. Hydrol. Reg. Stud.* **29**, 100690. https://doi.org/10.1016/j.ejrh.2020.100690 (2020).
53. Desai, S., Singh, D. K., Islam, A. & Sarangi, A. Multi-site calibration of hydrological model and assessment of water balance in a semi-arid river basin of India. *Quat Int.* **571**, 136–149. https://doi.org/10.1016/j.quaint.2020.11.032 (2021).

54. Serur, A. B. & Adi, K. A. Multi-site calibration of hydrological model and the response of water balance components to land use land cover change in a rift Valley lake basin in Ethiopia. *Sci. Afr.* **15**, e01093. https://doi.org/10.1016/j.sciaf.2022.e01093 (2022).
55. National Institute of Meteorological Research (NIMR). *Understanding of Climate Change II* (Seoul, 2009).
56. Petry, I. et al. Changes in flood magnitude and frequency projected for vulnerable regions and major wetlands of south America. *Geophys. Res. Lett.* **52** (5), e2024GL112436 https://doi.org/10.1029/2024GL112436 (2025).
57. Dysarz, T. et al. Assessment of climate change impact on flood hazard zones. *Water Resour. Manag.* **39** (2), 963–977. https://doi.org/10.1007/s11269-024-04002-8 (2025).
58. Yang, J. Q. & Nepf, H. M. Impact of vegetation on bed load transport rate and bedform characteristics. *Water Resour. Res.* **55**, 6109–6124. https://doi.org/10.1029/2018WR024404 (2019).
59. Sugianto, S., Deli, A., Miswar, E., Rusdi, M. & Irham, M. The effect of land use and land cover changes on flood occurrence in Teunom watershed, Aceh Jaya. *Land* **11**, 1271. https://doi.org/10.3390/land11081271 (2022).
60. Seemuangngam, A. & Lin, H. L. The impact of urbanization on urban flood risk of Nakhon ratchasima, Thailand. *Appl. Geogr.* **162**, 103152. https://doi.org/10.1016/j.apgeog.2023.103152 (2024).
61. Lompi, M., Mediero, L., Soriano, E. & Caporali, E. Climate change and hydrological dam safety: a stochastic methodology based on climate projections. *Hydrolo Sci. J.* **68** (6), 745–763. https://doi.org/10.1080/02626667.2023.2192873 (2023).
62. Hwang, J. & Lall, U. Increasing dam failure risk in the USA due to compound rainfall clusters as climate changes. *Npj Nat. Hazards.* **1**, 27. https://doi.org/10.1038/s44304-024-00027-6 (2024).
63. Döll, P., Douville, H., Güntner, A., Müller Schmied, H. & Wada, Y. Modelling freshwater resources at the global scale: challenges and prospects. *Surv. Geophys.* **37**, 195–221. https://doi.org/10.1007/s10712-015-9343-1 (2016).
64. Lee, S. et al. Flood vulnerability assessment of an urban area: A case study in seoul, South Korea. *Water* **15** (11), 1979. https://doi.org/10.3390/w15111979 (2023).
65. Teufel, B. et al. Investigation of the mechanisms leading to the 2017 Montreal flood. *Clim. Dyn.* **52**, 4193–4206. https://doi.org/10.1007/s00382-018-4375-0 (2019).
66. Philip, S. et al. Validation of a rapid attribution of the may/june 2016 Flood-Inducing precipitation in France to climate change. *J. Hydrometeor.* **19**, 1881–1898. https://doi.org/10.1175/JHM-D-18-0074.1 (2018).
67. Rogers, J. S., Maneta, M. M., Sain, S. R., Madaus, L. E. & Hacker, J. P. The role of climate and population change in global flood exposure and vulnerability. *Nat. Commun.* **16** (1), 1287 (2025).
68. Mayo, T. L. & Lin, N. Climate change impacts to the coastal flood hazard in the Northeastern united States. *Weather Clim. Extremes.* **36**, 100453. https://doi.org/10.1016/j.wace.2022.100453 (2022).
69. Wing, O. E. et al. Inequitable patterns of US flood risk in the anthropocene. *Nat. Clim. Change.* **12**, 2, 156–162. https://doi.org/10.1038/s41558-021-01265-6 (2022).
70. Arnell, N. W. & Gosling, S. N. The impacts of climate change on river flood risk at the global scale. *Clim. Change.* **134**, 387–401. https://doi.org/10.1007/s10584-014-1084-5 (2016).
71. Wasko, C., Nathan, R., Stein, L. & O'Shea, D. Evidence of shorter more extreme rainfalls and increased flood variability under climate change. *J. Hydrol.* **603**, 126994. https://doi.org/10.1016/j.jhydrol.2021.126994 (2021).
72. Tellman, B. et al. Satellite imaging reveals increased proportion of population exposed to floods. *Nature* **596**, 7870, 80–86. https://doi.org/10.1038/s41586-021-03695-w (2021).
73. Slater, L. J. & Villarini, G. Recent trends in US flood risk. *Geophys. Res. Lett.* **43**, 12–428 (2016).
74. Abbaspour, K. C. et al. Modelling hydrology and water quality in the pre-alpine/alpine Thur watershed using SWAT. *J. Hydrol.* **333**, 413–430. https://doi.org/10.1016/j.jhydrol.2006.09.014 (2007).
75. Nash, J. E. & Sutcliffe, J. V. River flow forecasting through conceptual models part I—A discussion of principles. *J. Hydrol.* **10**, 282–290. https://doi.org/10.1016/0022-1694(70)90255-6 (1970).
76. Gupta, H. V., Sorooshian, S. & Yapo, P. O. Status of automatic calibration for hydrologic models: Comparison with multilevel expert calibration. *J. Hydrol. Eng.* **4**, 135–143 (1999).
77. Sorooshian, S., Duan, Q. & Gupta, V. K. Calibration of rainfall-runoff models: application of global optimization to the Sacramento soil moisture accounting model. *Water Resour. Res.* **29**, 1185–1194. https://doi.org/10.1029/92WR02617 (1993).
78. Choi, Y. W. & Ahn, J. B. Impact of cumulus parameterization schemes on the regional climate simulation for the domain of CORDEX-East Asia phase 2 using WRF model. *Atmos* **27**, 1, 105–118 (2017). (In Korean with English abstract).
79. Jo, S. et al. The Köppen-Trewartha Climate-Type changes over the CORDEX-East Asia phase 2 domain under 2 and 3° C global warming. *Geophys. Resear Lett.* **46**, 23, 14030–14041. https://doi.org/10.1029/2019GL085452 (2019).
80. Lee, J. et al. Evaluation of the Korea meteorological administration advanced community Earth-System model (K-ACE). *Asia-Pacific J. Atmos. Sci.* **56**, 381–395. https://doi.org/10.1007/s13143-019-00144-7 (2020).
81. Kim, J. U. et al. Evaluation of performance and uncertainty for Multi-RCM over CORDEX-East Asia phase 2 region. *Atmos* **304**, 361–376. https://doi.org/10.14191/Atmos.2020.30.4.361 (2020). (in Korean with English abstract).
82. Kim, D. H. et al. Future projection of extreme climate over the Korean Peninsula using multi-RCM in CORDEX-EA phase 2 project. *Atmos* **31**, 5, 607–623. https://doi.org/10.14191/Atmos.2021.31.5.607 (2021). (in Korean with English abstract).
83. Kim, J. U. et al. Future climate projection in South Korea using the high-resolution SSP scenarios based on statistical downscaling. *J. Clim. Resear.* **17**, 2, 89–106. https://doi.org/10.14383/cri.2022.17.2.89 (2022). (In Korean with English abstract).
84. Kim, M. K. et al. Statistical downscaling for daily precipitation in Korea using combined PRISM, RCM, and quantile mapping: part 1, methodology and evaluation in historical simulation. *Asia-Pacific J. Atmos. Sci.* **52**, 2, 79–89. https://doi.org/10.1007/s13143-016-0010-3 (2016).
85. Kim, S. & Kim, M. K. Verification of PRIDE model version 2.0. *J. Clim. Resear.* **13** (1), 71–86. https://doi.org/10.14383/cri.2018.13.1.71 (2018). (in Korean with English abstract).
86. Cannon, A. J., Sobie, S. R. & Murdock, T. Q. Bias correction of GCM precipitation by quantile mapping: how well do methods preserve changes in quantiles and extremes? *J. Clim.* **28**, 17, 6938–6959. https://doi.org/10.1175/JCLI-D-14-00754.1 (2015).

Acknowledgements

This work was supported by the Korea Environment Industry &Technology Institute (KEITI) through the Climate Change R&D Project for the New Climate Regime. The study was funded by the Korean Ministry of Environment (MOE) (2022003570004). The work was supported by the National Research Foundation of Korea (NRF) grant funded by the Korean Government (MSIT)(No. RS-2023-00259403). The work was also supported by the Knowledge-Based Environmental Service Program funded by the Ministry of Environment.

Author contributions

A.B.A. conceptualized, compiled and analyzed the data of the manuscript with suggestions and contributions from J.K. Funding and extensive feedback was provided by J.K. All authors reviewed the manuscript.

Declarations

Competing interests
The authors declare no competing interests.

Additional information
Supplementary Information The online version contains supplementary material available at https://doi.org/10.1038/s41598-025-11921-y.

Correspondence and requests for materials should be addressed to J.K.

Reprints and permissions information is available at www.nature.com/reprints.

Publisher's note Springer Nature remains neutral with regard to jurisdictional claims in published maps and institutional affiliations.